Fast 2-photon stimulation using holographic patterns

Maia Brunstein[1], Jules Lubetzki[1], Cédric Moutoussamy[1,3], Wei Li[1], and Jérémie Barral[1,2,*]

[1]*Institut Pasteur, Université Paris Cité, INSERM, Institut de l'Audition, Paris, France*

[2]*CNRS, France*

[3]*Sorbonne Université, Paris, France*

**jeremie.barral@pasteur.fr*

Two decades after its introduction, optogenetics – a biological technique to control the activity of neurons or other cell types with light – remains a cutting edge and promising tool to study biological processes. Its increasing usage in research varies widely from causally exploring biological mechanisms and neural computations, to neurostimulation and sensory restauration. To stimulate neurons in the brain, a variety of approaches have been developed to generate precise spatiotemporal light patterns. Yet certain constrains still exists in the current optical techniques to activate a neuronal population with both cellular resolution and millisecond precision. Here, we describe an experimental setup allowing to stimulate a few tens of neurons in a plane at sub-millisecond rates using 2-photon activation. A liquid crystal on silicon spatial light modulator (LCoS-SLM) was used to generate spatial patterns in 2 dimensions. The image of the patterns was formed on the plane of a digital micromirror device (DMD) that was used as a fast temporal modulator of each region of interest. Using fluorescent microscopy and patch-clamp recording of neurons in culture expressing the light-gated ion channels, we characterized the temporal and spatial resolution of the microscope. We described the advantages of combining the LCoS-SLM with the DMD to maximize the temporal precision, modulate the illumination amplitude, and reduce background activation. Finally, we showed that this approach can be extended to patterns in 3 dimensions. We concluded that the methodology is well suited to address important questions about the role of temporal information in neuronal coding.

Introduction

A fundamental question in neuroscience is to understand how patterns of neuronal activity can represent useful sensory or motor information to drive relevant animal behavior. To build a causal link between brain activity and behavior, it is necessary to control the neuronal dynamics and observe how animal comportment is affected (Panzeri, Harvey et al. 2017). Addressing this challenge requires tools to manipulate a population of neurons in a very controlled manner. This can now be achieved by optogenetics, a genetic manipulation that modifies neurons to make them sensitive to light (Yizhar, Fenno et al. 2011). Neurons expressing the light gated ion channel channelrhodopsin can be activated by brief light pulses. Combined with diverse optical methods to produce precise light patterns, it allows to specifically activate a defined ensemble of neurons (Ronzitti, Ventalon et al. 2017, Chen, Papagiakoumou et al. 2018).

Because neurons are embedded in the diffractive brain tissue, 2-photon (2P) activation is often necessary to reach cells in deep structures with single-cell resolution. Two classes of strategies have been developed to stimulate neurons using 2P activation. A first possibility is to scan a femtosecond infrared laser beam onto target cells using galvanometric mirror (Rickgauer and Tank 2009) or optoacoustic deflectors (Ricci, Marchetti et al. 2022). However, this approach is still too slow to activate a large population of neurons with good temporal precision, especially in 3 dimensions.

The optimal choice for stimulating simultaneously several cell targets is to benefit from non-scanning methods (Papagiakoumou, Anselmi et al. 2010, Papagiakoumou, Ronzitti et al. 2018), such as holography which enables to generate arbitrary patterns in 3 dimensions. However, using this technique alone to update temporal patterns rapidly is limited by two major bottlenecks. First, the refresh rate of the fastest Liquid Crystal on Silicon Spatial Light Modulator (LCoS-SLM) on the market is effectively limited to about 300-400 Hz because liquid crystals have a rise time of ~2 ms when used with infrared wavelengths. Therefore, better temporal precision cannot be achievable in this configuration. Second, if for example we need to stimulate few tens of targets with random temporal patterns during 1 s, one can reasonably assume that each pattern of the sequence will be different. Thus, one will need to build about 500 phase patterns. Although this is feasible to pre-build the patterns and store them either on a computer or on the onboard memory of the device, it precludes any real-time control of neuronal activity because of the necessary computational time to calculate these patterns with the Gerchberg-Saxton iterative algorithm (Gerchberg and Saxton 1972).

Considering 1P stimulation, one simple approach is to use a spatial light modulator in a plane conjugated with the sample plane and modulate the amplitude of the light (Ronzitti, Ventalon et al. 2017). Because Digital Micromirror Devices (DMD) can achieve binary frame rates up to 10 kHz, they have been successfully employed to activate an arbitrary number of targets with sub-millisecond precision (Barral and Reyes 2016, Barral and Reyes 2017). However, the intensity of each pixel is, in this case, the intensity of

the light source divided by the total number of pixels. Taking a very conservative approach, if one is able to bring 10 W of light to the sample, one cannot expect more than 10 µW of light per pixel with a DMD of 1000x1000 pixels. With a pixel size on the sample of 0.5 µm (considering a 20X magnification and a 10 µm pixel size on the DMD), it represents 40 $\mu W \cdot \mu m^{-2}$. This is clearly enough for 1P stimulation where the saturating activation of channelrhodospin ChR2 is usually around 0.01 $\mu W \cdot \mu m^{-2}$, but this only allows to activate a small fraction of opsins with 2P stimulation. To overcome these limitations, we used a LCoS-SLM to generate a single spatial pattern in 2 or 3 dimensions containing multiple regions of interest and projected this pattern onto a DMD that was employed as a fast temporal shutter for each region of interest. In this way, the total laser power was efficiently dedicated to activating only potential targets without wasting laser power on unused DMD pixels. This approach had been applied to imaging application with the development of an encoded multisite 2P microscope (Ducros, Goulam Houssen et al. 2013). The main advantages of our optical developments are (i) to push the temporal resolution to the limitations of the opsin time constant, (ii) to reduce the complexity of the phase pattern calculation since only 1 phase pattern needs to be built, (iii) to enable real-time control of neuronal activity. We further demonstrate that the set-up also enables stimulation in 3 dimensions.

Methods

Microscope apparatus

To achieve a precise control of the light pattern both temporally and spatially, we developed a homemade high-speed photo-stimulation system coupled to a 2-photon microscope (Fig 1). For the 2-photon microscope, the excitation beam (920nm, Opera HP, Coherent) was expanded through a beam expander and sent to a scanning galvanometer mirror (GVSM002/M, Thorlabs). After the scanner, the beam impinged the scan lens (LSM04-BB, Thorlabs) followed by the tube lens to be finally focalized by the 20X objective (XLUMPLFLN20XW, Olympus). The emission of the sample was collected with the same objective and sent via a dichroic filter (DMLP735B, Thorlabs) through the de-scan lens to the PMT detector (PMT2101/M, Thorlabs). In order to find the region of interest on the focal plane, we added an epi-fluorescence system, composed by a 470nm LED, a 469/35 excitation filter, a 500LP dichroic, and a 525/40 emission filter. Because our laser for 2P microscopy had a low repetition rate (2 MHz), we synchronized the acquisition of the fluorescent signal with the laser pulses to correct the fluorescent signal within each pixel by the actual number of laser pulses. To do so, we built a custom user interface programmed with LabVIEW (National Instrument) that controlled the whole microscope apparatus described here.

In the photostimulation path, the emission of the laser (1035nm, Monaco, Coherent) was expended to fill the sensitive area of the LCoS-SLM (E-series 1920x1200 pixels, Meadowlarks optics). The LCoS-SLM allowed modifying the phase of the incident beam at the back focal plane of the objective in order to create

an arbitrary intensity pattern on the image plane (i.e. several diffracted limited spots in 3D, large patterns or arbitrary shapes). A blocking mask in a conjugated image plane was used to block the 'zero order' of the LCoS-SLM (non-modulated light). To be able to modify the illumination at high speed, we projected the intensity pattern created by the LCoS-SLM onto a DMD (DLP650LNIR, Texas Instruments) controlled by a third-party controller (V-650L, Vialux) to achieve full-frame temporal modulation above 10 kHz. Finally, the phase-modulated beam was combined with the two-photon excitation beam with a 1020 nm short-pass dichroic mirror (DMSP1020B, Thorlabs) before going through the tube lens and the objective and being projected on the sample plane.

To characterize the spatiotemporal properties of the optical setup, we visualized 2D patterns generated onto a fluorescent microscope slide (Chroma) placed at the sample plane and imaged through the fluorescent light path by a rapid camera (ORCA-Flash4.0, Hamamatsu).

To reconstruct 3D patterns, a visualization system composed of an additional 20X air objective, a 150 mm focal length tube lens and a CCD camera was positioned under the sample. In this case, the sample was a thin layer of fluorescent ink enclosed between a slide and a coverslip. This configuration was used to visualize the 3D illumination patterns as well as the intensity profile of the stimulation spot in X-Y-Z.

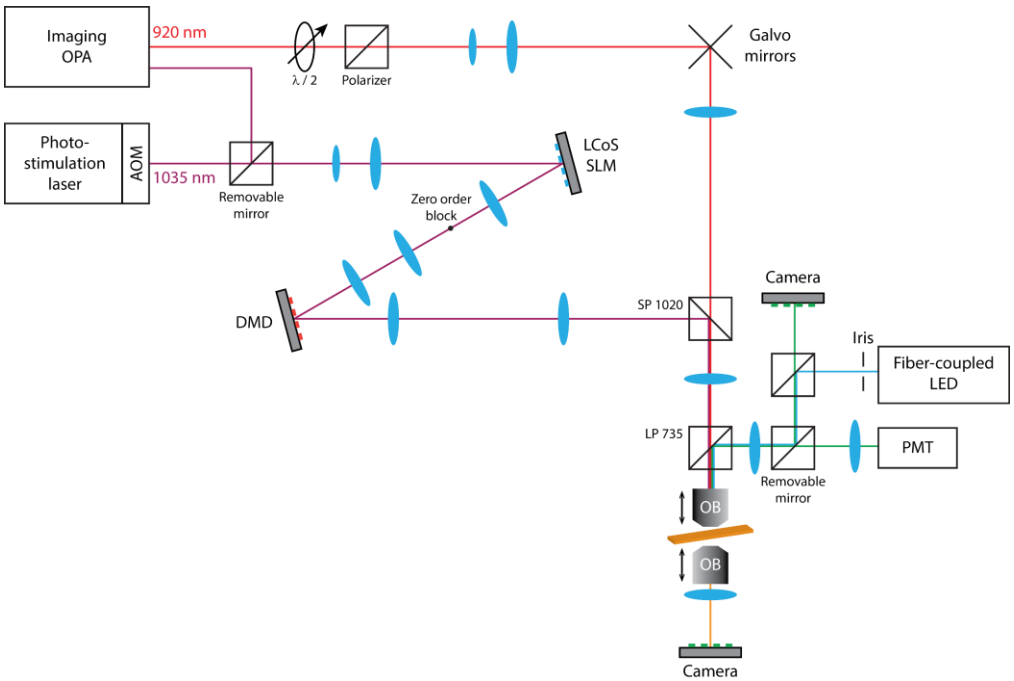

Fig. 1. Optical light paths of the 2-photon microscope and 2-photon stimulation device. The 920 nm laser was scanned on the sample plane trough the objective by the galvanometer mirrors. The fluorescence emission was collected by the same objective and sent to the PMT. The phase of the 1035 nm laser was modulated by the LCoS-SLM to form an arbitrary pattern on the DMD surface. This last element was used as a fast temporal shutter to excite different regions of interest on the sample plane with high temporal resolution. A second objective was placed under the sample to image patterns in 3D.

Calibration

The system was calibrated before each use to match the image from the camera (top camera) with both the LCoS-SLM and DMD projection units and the image from the 2P microscope. For simplicity, the image from the camera was considered as the reference. To calibrate the LCoS-SLM, a phase mask was sent from the LCoS-SLM to create a grid of 4x4 spots while the DMD was in an all-ON configuration. Spots generated by the LCoS-SLM were detected on the camera and a geometric matching algorithm (Vision Development Module, LabView, National Instruments) was used to calibrate for perspective or nonlinear distortion errors. To calibrate the DMD, the LCoS-SLM sent a white pattern to the DMD which was configured to create a grid of 4x4 spots. Finally, the 2P imaging path was calibrated by sending spots sequentially at different locations using fixed angle deflections with the galvanometer mirrors.

Neuronal cultures and electrophysiology

Dissociated cortical neurons from postnatal (P0-P1) mice were prepared as described previously (Hilgenberg and Smith 2007, Barral and Reyes 2016, Barral and Reyes 2017) and in accordance with French and European regulations for the care and protection of laboratory animals (EC Directive 2010/63, French Law 2013–118). Briefly, the mouse cortex of FVB wild type mice (Janvier Laboratory) was dissected in cold CMF-HBSS (Ca^{2+} and Mg^{2+} free Hank's balanced salt solution containing 1 mM pyruvate,15 mM HEPES, 10 mM $NaHCO_3$). The tissue was dissociated in papain (15 U/mL, Roche) containing 1 mM L-cystein, 5 mM 2-amino-5-phosphonopentanoic acid and 100 U/ml DNase (DN25, Sigma) for 25 min. After enzymatic inactivation in CMF-HBSS containing 100 mg/mL BSA (A9418, Sigma) and 40 mg/mL trypsin inhibitor (T9253, Sigma), pieces were mechanically dissociated with a pipette and plated on a glass coverslip. Before plating, glass was cleaned in 3 N HCl for 48 h and immersed in sterile aqueous solution of 0.1 mg/mL poly-L-lysine (P4707, Sigma) for 12 h. Neurons were grown in Neurobasal medium (supplemented with B27, Glutamax and penicillin/streptomycin cocktail, Gibco) in a humidified incubator at 37 °C, 5% CO_2. One third of the culture medium was exchanged every 3 days.

Expression of channelrhodopsin (ChR2) was achieved by viral infection with AAV2-hSyn-hChR2(H134R)-EYFP of cortical neurons. The virus was produced at 3×10^{12} cfu/mL by the University of Pennsylvania Vector Core using plasmid provided by Karl Deisseroth (Stanford University). At 3 days *in vitro* (DIV), the culture was infected with 1 µL of virus. Experiments were performed at 14-21 DIV, when neuronal characteristics and network connectivity were mature and expression of ChR2 was sufficient to enable reliable photostimulation.

Recordings were performed at room temperature in artificial cerebrospinal fluid (aCSF). The aCSF solution contained (in mM): 125 NaCl, 15 $NaHCO_3$, 25 D-glucose, 10 HEPES, 2.5 KCl, 2 $CaCl_2$, 1.25 NaH_2PO_4 and 1 $MgCl_2$. Electrodes, pulled from borosilicate pipettes (1.5 OD) on a Flaming/Brown micropipette puller (Sutter Instruments), had resistances in the range of 6-10 MΩ when filled with internal solution

containing (in mM): 130 K-gluconate, 10 HEPES, 10 phosphocreatine, 5 KCl, 1 $MgCl_2$, 4 ATP-Mg and 0.3mM GTP.

Cells were visualized through the water-immersion objective and fluorescence microscopy was used to confirm ChR2 expression. Whole-cell current-clamp recordings were made using Intan CLAMP amplifier (Intan Technologies). The signal was filtered at 10 kHz and digitized at 50 kHz.

Results

Microscope design and pattern quality

The 2P stimulation path of the microscope was based on a fixed-wavelength femtosecond laser at 1035 nm capable of delivering a power of 40 W (Fig. 1). The laser beam was expanded onto the LCoS-SLM and the zero-order diffraction was physically eliminated. The image was then projected onto the DMD and further relayed to the sample plane. Several calibration steps were necessary to find the corresponding locations of pixels on the LCoS-SLM, DMD, camera, and 2P scanning image (see Methods). Once calibrated, the user defined Regions of Interest (ROIs). A unique phase mask containing all the ROIs was generated using the Gerchberg-Saxton iterative algorithm (Gerchberg and Saxton 1972) and projected by the LCoS-SLM. A collection of corresponding masks on the DMD were also designed. Each mask defined whether each ROI was sent or not to the sample. The DMD was thus used as a switchable mirror for each region of interest. Because theses masks were simply 1-bit images, they could be pre-built or generated in real-time.

Some concerns could be raised whether the introduction of a grid of micromirrors could degrade the quality of patterns generated by the LCoS-SLM. We measured the intensity profile in 3 dimensions of an 8 µm diameter disk generated by the LCoS-SLM when all mirrors of the DMD where in ON position (Fig. 2a) or when only the mirrors corresponding to the ROI were reflecting the optical pattern (Fig. 2b). Both in the sample plane or in a plane containing the optical axis, the different configurations provided similar shapes. These intensities profiles are also similar to those found in the literature using only a LCoS-SLM (Papagiakoumou, Anselmi et al. 2010).

Interestingly, the use of the DMD allowed a sharper transition between the ROI and the background on the XY plane with slightly more light within a ROI than outside (Fig. 2c). To fully characterize the amount of light projected to the desired area, we quantified the contrast ratio defined as the average pixel intensity within a ROI divided by the average background intensity. When the pattern contained only a single ROI, the contrast ratio was 157:1 and was actually improved by 27% when the DMD allowed to reflect only the corresponding ROI (Table 1). This is because the spatial pattern defined by the LCoS-SLM was not perfect and light is also diffracted to unwanted regions. The DMD permitted to remove part of this diffracted light. Concurrently, it decreased the brightness of the pattern by 15% but this remains acceptable as actual laser are usually able to provide sufficient power for biological applications. When the pattern contained 10 ROIs

with the same input power, the contrast ratio was decreased to 18:1 but again could be increased significantly when a pattern corresponding to the 10 ROIs was displayed on the DMD instead of a totally reflective pattern.

Along the axial direction, patterns were also more confined with the use of the DMD (Fig. 2d). This can be seen as the smaller width along the Z axis: on average, the full width at half maximum decreased from 21.0 ± 0.3 to 20.0 ± 0.3 µm (mean ± SE, n = 10). A thickness of about 20 µm (Fig. 2) is very comparable to published data (Papagiakoumou, Anselmi et al. 2010) but could notably be reduced with the introduction of temporal focusing (Papagiakoumou, Ronzitti et al. 2020). We did not use this technique in the present study, but it would be adaptable to our optical design and would help to decrease this value if needed.

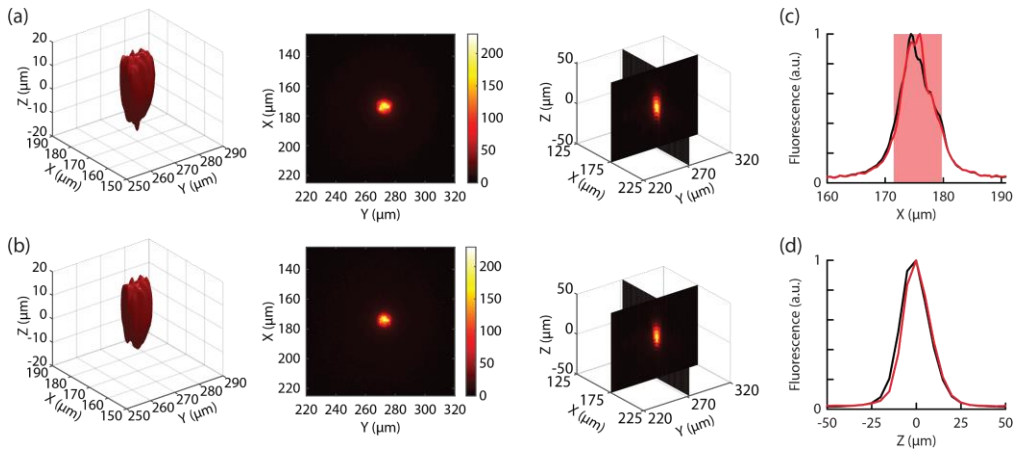

Fig. 2. Profile of an optical pattern when all mirrors of the DMD where in the ON position (a) or when only the mirrors corresponding to the ROI where ON (b). 3-dimensional reconstruction of a stimulation volume with an isosurface corresponding to 20% of the maximal amplitude (left). Intensity profiles of the stimulation volume in the XY plane (middle) and in the planes along the optical axis (right). (c) Intensity profile along the X axis when all the mirrors of the DMD were in the ON position (black) or when only the mirrors corresponding to the ROI were ON (red). (d) Same as in (c) for the intensity profile along the Z axis.

Table 1. Contrast between the fluorescence within an ROI and the background

	Contrast ratio without DMD patterns (C_0)	Contrast ratio with DMD patterns (C_{DMD})	Increase in contrast ratio (C_{DMD}/C_0)
1 ROI	157 ± 14	205 ± 36	1.27 ± 0.11
10 ROIs	18.4 ± 0.71	19.5 ± 0.7	1.06 ± 0.01

Fast 2-photon stimulation

To assess the temporal characteristics of the stimulation, we used a rapid camera to image a fluorescent sample. In a first experiment, we reduce the field of view of the CMOS camera to several lines to achieve a frame rate of 10 kHz that matched the DMD framerate. We built a phase mask to generate 6 ROIs that

were successively illuminated for 1 ms via updating the corresponding patterns on the DMD (Fig. 3a). This enabled us to verify that the temporal resolution of the set-up was only limited by the frame rate of the DMD and that no cross-illumination was generated by introducing the DMD between the LCoS-SLM and the objective.

In a second experiment, we increased the number of ROIs to 20 to make it more realistic regarding brain stimulation. The frame rate was decreased to 1 kHz to increase the field of view of the camera and the stimulation duration was set to 5 ms for each ROI (Fig. 3b). However, the DMD was still displaying patterns at 10 kHz and onsets had thus a 0.1 ms resolution. Also in this case, each ROI was faithfully activated without cross-illumination.

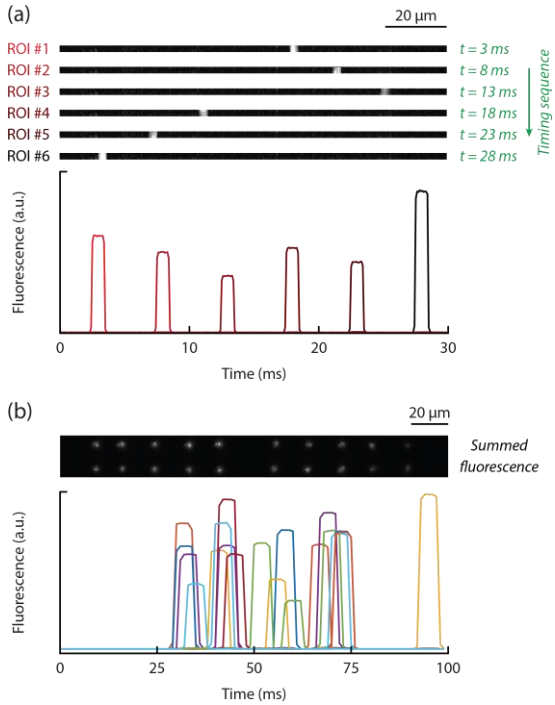

Fig. 3. Temporal characterization of optical stimulation. (a) 6 ROIs illuminated consecutively for 1 ms by updating the DMD patterns (DMD and camera framerates: 10 kHz). Each image shows the fluorescence at a single point in time indicated in green on the right. Bottom graph shows the fluorescence signal of each ROI as a function of time. (b) 20 ROIs illuminated consecutively for 5 ms by updating the DMD pattern (DMD framerate 10 kHz and camera framerate 1 kHz). The fluorescent image shows here the average light intensity during the duration of a whole sequence. Bottom graph shows the fluorescence signal of each ROI as a function of time.

The DMD can also be used as an amplitude modulator. To obtain the maximal intensity, all mirrors are turned ON within a single ROI. However, one can select only a fraction of mirrors (Fig. 4a) and update the identity of ON mirrors at every frame to maintain an average illumination intensity while varying the illuminated regions inside the ROI. In this case, the ROI receives a fraction of light. This approach is of

course applicable only if the biological process under study is slower than the DMD framerate (> 10 kHz), which is often the case.

We verified this by increasing the fraction of ON mirrors on a single ROI while measuring the average fluorescence of the ROI shape on the camera (Fig. 4b, left). The relation between the average fluorescence and the fraction of ON mirrors was monotonic but nonlinear (Fig. 4b, right) because the size of a single DMD mirror on the sample plane (~500 nm) is on the same order of magnitude than the microscope resolution. Thus, neighboring mirrors were not independent and 2P nonlinear effects were still present. However, a proper calibration permits to target the exact desired light intensity.

Using either a camera (Fig. 4c) or the PMT (Fig. 4d) to collect the average fluorescence intensity of the whole ROI, we established that a sinusoidal modulation of light intensity was possible up to the kHz frequency range. Taken together, this shows that this strategy enables to stimulate independently and with varying intensities an arbitrary number of ROIs with a frame rate only limited by the refresh rate of the DMD.

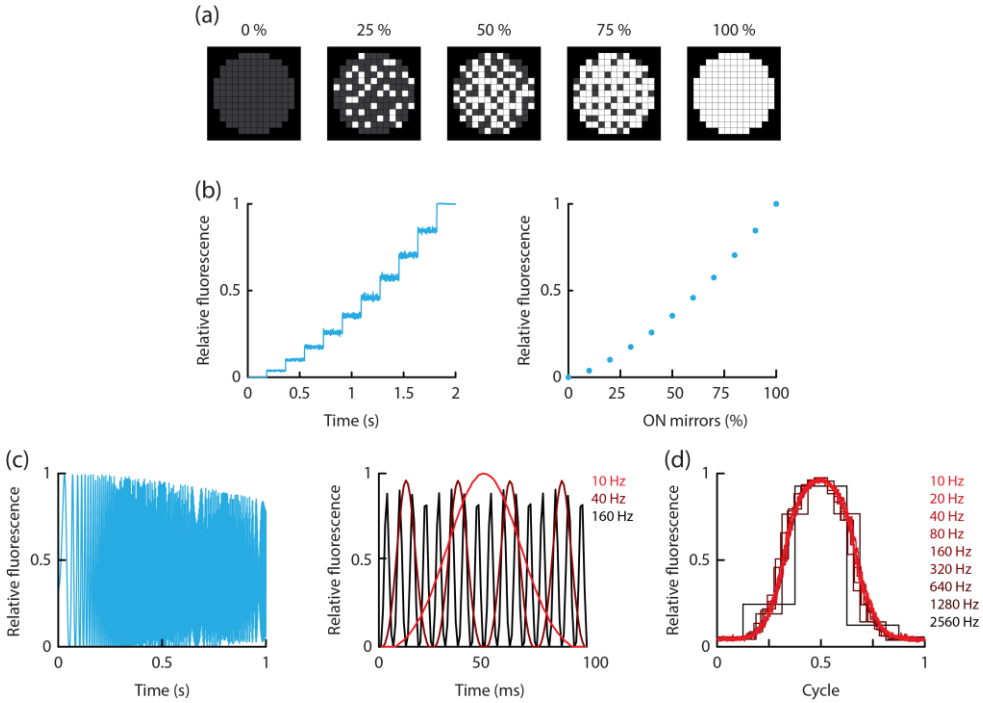

Fig. 4. Using the DMD as a fast amplitude modulator. (a) Examples of DMD patterns with variable fractions of ON mirrors in order to modulate the average illumination amplitude of a single ROI. (b) Step modulation. Relative fluorescence (left) measured on the ROI using the camera as a function of time when an increasing fraction of mirrors on the DMD were turned ON. The average fluorescence was calculated during each step and plotted as a function of percentage of ON mirrors (right). (c) Frequency modulation measured with the camera. Chirp response for a modulating frequency varying between 1 and 500 Hz (left). Examples of sinusoidal modulation for 3 frequencies and plotted as a function of time. (d) Frequency modulation measured with the PMT and plotted as a function of cycle to display the frequency limit of the device. Note that all temporal traces displayed here were not averaged and correspond single trials.

Modulation of 3D patterns

In this section, we extend our stimulation method to patterns in 3 dimensions. To target 4 different planes, we divided the grid of the LCoS-SLM in 4 sub-grids that were each targeting a different plane (Z = 55, 110, 195, 250 µm). Pixels from each sub-array were uniformly distributed to maximize homogeneity of the light source intensity. Although, our approach is based on conjugating the amplitude pattern produced by the LCoS-SLM with the plane of the DMD, it is still possible to modulate a ROI even if it is not in the plane of the DMD as long as the ROIs were not too close. To do so, we designed ROIs on the DMD that had a diameter of about 30 µm compared to the 8 µm of the actual target. Compared to a case where all the mirrors of the DMD are ON (Fig. 5a), the pattern quality was not significantly affected when only mirrors corresponding to the different ROIs where ON (Fig. 5b). Thus, we could selectively erase 1 or more ROIs (Fig. 5c-d) even if the image generated by the LCoS-SLM is out of the DMD focus. Importantly, the selective modulation of the patterns in 3D could be done at the DMD framerate.

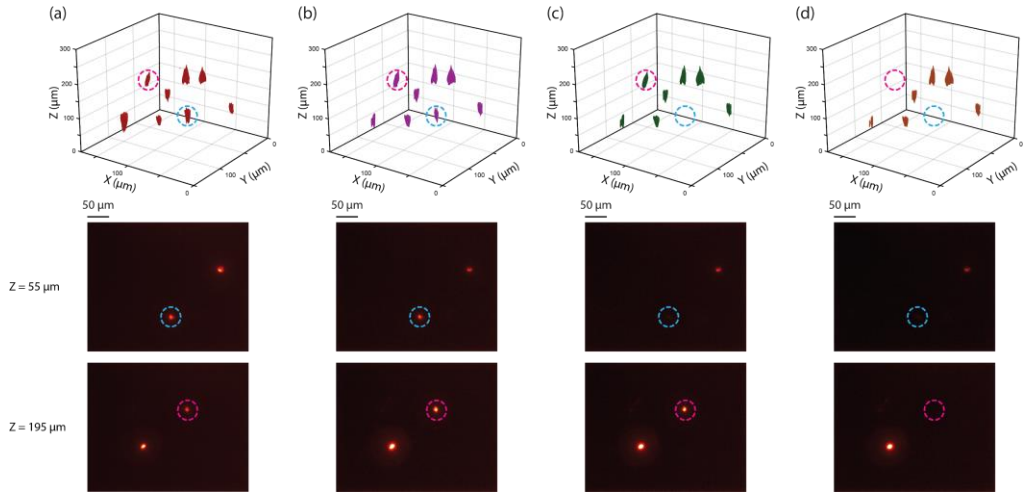

Fig. 5. Selective modulation of patterns in 3 dimensions. (a) 3-dimensional reconstruction (top) of the optical patterns when all the mirrors of the DMD where in the ON position. Two selected planes are shown (bottom). (b-d) Same as in (a) when only the mirrors corresponding to the 8 ROIs where ON (b) or when only 7 (c) or 6 (d) ROIs were ON on the DMD.

Physiological assessment of spatiotemporal characteristics

To characterize our stimulation method functionally, we grew primary cortical neurons onto a glass coverslip and expressed the light-gated ion channel channelrhodpsin ChR2(H134R) using viral transfection (see Methods). We monitored membrane potential using patch-clamp recordings (Fig. 6a). Cells had intrinsic properties similar to published data (Table 2) (Barral and Reyes 2016). We stimulated neurons either using 2P light patterning as described above or with the fiber-coupled LED of the 1P fluorescent light path where an iris was placed on the conjugated plane of the sample (Fig. 1). Upon light activation, light-sensitive channels on the neuron's membrane open, leading to a photocurrent and thus neuron's depolarization from its resting membrane potential (Fig. 6b). Neurons were significantly more depolarized

using 1P than with 2P stimulation (Table 2), which was expected since ChR2 is not optimized for 2P stimulation. Recent advances in biochemical engineering have now permitted to produce much more efficient opsins for 2P activation both in terms of kinetics and photocurrent (Sridharan, Gajowa et al. 2022). Here, we used this approach to describe only the spatial resolution of the setup because the slow kinetics of the opsin did not permit to fully appreciate the fast temporal performances of the microscope. We measured the depolarization of single neurons as a function of the position of the stimulation pattern. Depolarization dropped by 50% when the stimulation region was moved within the sample plane by about 54 µm and 32 µm for 1P and 2P stimulation, respectively (Fig. 6c-d). Note that the lower resolution for 1P stimulation is mainly due to the iris size that had a diameter of about 60 µm on the sample plane, compared to the 15 µm spot diameter that were generated with the LCoS-SLM. Upon 2P stimulation, depolarization was decreased by 50% when the focus was moved away by 34 µm (Table 2, Fig. 6c-e), a value very comparable to published data using conventional holography (Pegard, Mardinly et al. 2017). Notably, these profiles could be substantially sharpened along the optical axis using temporal focusing (Andrasfalvy, Zemelman et al. 2010, Papagiakoumou, Anselmi et al. 2010, Pegard, Mardinly et al. 2017).

Table 2. Electrophysiological characterization of neuron intrinsic properties and light stimulation

	V_m (mV)	R (MΩ)	C (pF)	ΔV 1P (mV)	ΔV 2P (mV)	FWHM in Z (µm)
Mean ± SE	-62.3 ± 2.6	245 ± 33	55.7 ± 5.9	14.4 ± 1.2	5.6 ± 0.6	66.9 ± 3.7
n	14			22	19	

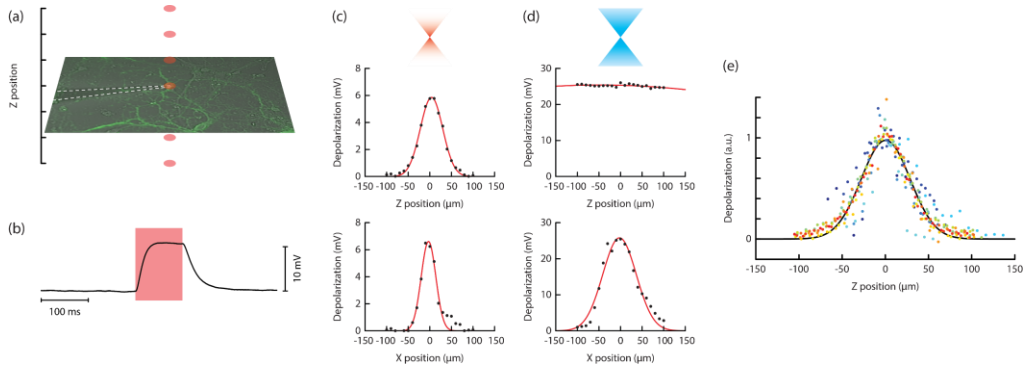

Fig. 6. Functional characterization of the spatial precision of holographic stimulation. (a) Experimental design where patch-clamp recording was made from a cortical neuron in culture. (b) Example data of a depolarizing step upon 2P activation. (c-d) Steady voltage depolarization as a function of the axial (top) and lateral (bottom) position of the stimulation spot for 2P (c) and 1P (d) stimulations. Except for 1P axial sensitivity, experimental data points were fitted by a Gaussian curve. (e) Population data showing the normalized voltage depolarization as a function of the axial position of the stimulation spot for 2P activation (n = 19 neurons). For each individual neuron, fit parameters were used to normalize the maximal depolarization to 1 and center the Gaussian curve to Z = 0. An axial precision of 67 µm (FWHM) for a spot of 15 µm diameter was found.

Discussion

Need for temporal resolution

A temporal resolution of 0.1 ms might not seem necessary at first sight because neuronal spike latency upon light stimulation is usually around 3-6 ms (Yizhar, Fenno et al. 2011, Ronzitti, Conti et al. 2017, Mardinly, Oldenburg et al. 2018, Sridharan, Gajowa et al. 2022). However, spike timing precision is well below latency values. Using the high-speed variant opsin Chronos, fast spiking interneurons could trigger spikes with a temporal precision of 0.2 ms upon 2P activation (Ronzitti, Conti et al. 2017). Sub-millisecond time jitter was also achieved with the newly developed opsin family ChroME (Mardinly, Oldenburg et al. 2018, Sridharan, Gajowa et al. 2022). ChroME variants have activation spectra centered around 1000 nm, a slightly higher wavelength than Chronos, which make them ideal for stimulation using Yb:YAG fiber lasers that can provide the necessary power to target a large number of cells in parallel and study how spatiotemporal patterns of neuronal activation are both necessary and sufficient for encoding information in the brain.

Spike timing with millisecond precision is important in many physiological processes such as spike-timing dependent plasticity (Bi and Poo 1998), song generation in the bird song (Hahnloser, Kozhevnikov et al. 2002), sensory processing (Rose, Brugge et al. 1967), or hippocampal memory replay (Carr, Jadhav et al. 2011). With the aim at reproducing precise neuronal sequences, our approach coupled to newly developed opsins provides a valuable resource to tackle fundamental questions about the role of temporal information in neuronal coding.

Extension to 3D patterns

The ability to produce patterns in 3 dimensions is important for applications in biological tissues. An axial resolution of the 2P stimulation of the order of 67 µm for a spot of 15 µm diameter was found. This value could be reduced to ~10 µm with the addition of temporal focusing technique described in several studies (Andrasfalvy, Zemelman et al. 2010, Papagiakoumou, Anselmi et al. 2010, Pegard, Mardinly et al. 2017). It is thus expected that the single cell resolution can be achieved in complex biological tissues. This resolution is often necessary when dealing with specimens in 3 dimensions to avoid unwanted cross-activations.

Previous approaches used either holography (Pegard, Mardinly et al. 2017), tunable lenses (Yang, Carrillo-Reid et al. 2018) or AOD (Ricci, Marchetti et al. 2022) to target different planes, all of which did not provide a sufficient temporal resolution to activate a large population of neurons in 3D simultaneously or with precise temporal patterns. Our optical design alleviates this limitation by using the DMD as a temporal modulator of each ROI independently. For 3D applications, we showed that temporal patterns could be modulated as long as the different patterns are not aligned along the Z axis. Here, we were able to control

specifically individual ROIs from different planes that were separated by up to 200 µm which represents a volume relevant for the study of cortical processes for example.

Acknowledgments

We thank Nicolas Michalski and Boris Gourévitch for lending us the CMOS camera and Brice Bathellier for the virus sample. This work was supported by a Human Frontier Science Program Career Development Award (CDA00009/2017-3), by the CNRS Momentum program and by the Fondation pour l'Audition (FPA IDA01). We acknowledge the support of the Fondation pour l'Audition to the Institut de l'Audition.

Disclosures

The authors declare that their principal affiliations are with not-for-profit organizations and that they have no potential conflict of interest in the publication of this article.

Data availability

The data that support the findings of this study are not publicly available at this time but may be obtained from the corresponding authors upon reasonable request. Data acquisition (Labview) and analysis (Labview or Matlab) software used in this paper are described in the Methods and will be available upon request.

References

Andrasfalvy, B. K., B. V. Zemelman, J. Tang and A. Vaziri (2010). "Two-photon single-cell optogenetic control of neuronal activity by sculpted light." Proc Natl Acad Sci U S A **107**(26): 11981-11986.

Barral, J. and A. D. Reyes (2016). "Synaptic scaling rule preserves excitatory-inhibitory balance and salient neuronal network dynamics." Nat Neurosci **19**(12): 1690-1696.

Barral, J. and A. D. Reyes (2017). "Optogenetic Stimulation and Recording of Primary Cultured Neurons with Spatiotemporal Control." Bio Protoc **7**(12).

Bi, G. Q. and M. M. Poo (1998). "Synaptic modifications in cultured hippocampal neurons: dependence on spike timing, synaptic strength, and postsynaptic cell type." J Neurosci **18**(24): 10464-10472.

Carr, M. F., S. P. Jadhav and L. M. Frank (2011). "Hippocampal replay in the awake state: a potential substrate for memory consolidation and retrieval." Nat Neurosci **14**(2): 147-153.

Chen, I. W., E. Papagiakoumou and V. Emiliani (2018). "Towards circuit optogenetics." Curr Opin Neurobiol **50**: 179-189.

Ducros, M., Y. Goulam Houssen, J. Bradley, V. de Sars and S. Charpak (2013). "Encoded multisite two-photon microscopy." Proc Natl Acad Sci U S A **110**(32): 13138-13143.

Gerchberg, R. W. and W. O. Saxton (1972). "Practical Algorithm for Determination of Phase from Image and Diffraction Plane Pictures." Optik **35**(2): 237-+.

Hahnloser, R. H., A. A. Kozhevnikov and M. S. Fee (2002). "An ultra-sparse code underlies the generation of neural sequences in a songbird." Nature **419**(6902): 65-70.

Hilgenberg, L. G. and M. A. Smith (2007). "Preparation of dissociated mouse cortical neuron cultures." J Vis Exp(10): 562.

Mardinly, A. R., I. A. Oldenburg, N. C. Pegard, S. Sridharan, E. H. Lyall, K. Chesnov, S. G. Brohawn, L. Waller and H. Adesnik (2018). "Precise multimodal optical control of neural ensemble activity." Nat Neurosci **21**(6): 881-893.

Panzeri, S., C. D. Harvey, E. Piasini, P. E. Latham and T. Fellin (2017). "Cracking the Neural Code for Sensory Perception by Combining Statistics, Intervention, and Behavior." Neuron **93**(3): 491-507.

Papagiakoumou, E., F. Anselmi, A. Begue, V. de Sars, J. Gluckstad, E. Y. Isacoff and V. Emiliani (2010). "Scanless two-photon excitation of channelrhodopsin-2." Nat Methods **7**(10): 848-854.

Papagiakoumou, E., E. Ronzitti, I. W. Chen, M. Gajowa, A. Picot and V. Emiliani (2018). Two-Photon Optogenetics by Computer-Generated Holography. Optogenetics: A Roadmap**:** 175-197.

Papagiakoumou, E., E. Ronzitti and V. Emiliani (2020). "Scanless two-photon excitation with temporal focusing." Nat Methods.

Pegard, N. C., A. R. Mardinly, I. A. Oldenburg, S. Sridharan, L. Waller and H. Adesnik (2017). "Three-dimensional scanless holographic optogenetics with temporal focusing (3D-SHOT)." Nat Commun **8**(1): 1228.

Ricci, P., M. Marchetti, M. Sorelli, L. Turrini, F. Resta, V. Gavryusev, G. Vito, G. Sancataldo, F. Vanzi, L. Silvestri and F. S. Pavone (2022). "Power-effective scanning with AODs for 3D optogenetic applications." Journal of Biophotonics **15**(4): e202100256.

Rickgauer, J. P. and D. W. Tank (2009). "Two-photon excitation of channelrhodopsin-2 at saturation." Proc Natl Acad Sci U S A **106**(35): 15025-15030.

Ronzitti, E., R. Conti, V. Zampini, D. Tanese, A. J. Foust, N. Klapoetke, E. S. Boyden, E. Papagiakoumou and V. Emiliani (2017). "Sub-millisecond optogenetic control of neuronal firing with two-photon holographic photoactivation of Chronos." J Neurosci.

Ronzitti, E., C. Ventalon, M. Canepari, B. C. Forget, E. Papagiakoumou and V. Emiliani (2017). "Recent advances in patterned photostimulation for optogenetics." Journal of Optics **19**(11).

Rose, J. E., J. F. Brugge, D. J. Anderson and J. E. Hind (1967). "Phase-locked response to low-frequency tones in single auditory nerve fibers of the squirrel monkey." J Neurophysiol **30**(4): 769-793.

Sridharan, S., M. A. Gajowa, M. B. Ogando, U. K. Jagadisan, L. Abdeladim, M. Sadahiro, H. A. Bounds, W. D. Hendricks, T. S. Turney, I. Tayler, K. Gopakumar, I. A. Oldenburg, S. G. Brohawn and H. Adesnik (2022). "High-performance microbial opsins for spatially and temporally precise perturbations of large neuronal networks." Neuron **110**(7): 1139-1155.e1136.

Yang, W., L. Carrillo-Reid, Y. Bando, D. S. Peterka and R. Yuste (2018). "Simultaneous two-photon imaging and two-photon optogenetics of cortical circuits in three dimensions." Elife **7**.

Yizhar, O., L. E. Fenno, T. J. Davidson, M. Mogri and K. Deisseroth (2011). "Optogenetics in neural systems." Neuron **71**(1): 9-34.